New Physics: Sae Mulli,
Vol. 70, No. 2, February 2020, pp. 108∼113
http://dx.doi.org/10.3938/NPSM.70.108

A Study of the Thermal Properties of Nano-crystalline Binary Oxides Prepared by Co-precipitation Method

Tahira Amer Bashir Ziya
Department of Physics, B. Z. University, Multan 60800, Pakistan

Muhammad Naeem Ashiq
Institute of Chemical Sciences, B. Z. University, Multan 60800, Pakistan

Jae-Hyeon Ko*
School of Nano Convergence Technology, Nano Convergence Technology Center, Hallym University, Chuncheon 24252, Korea

Farooq Bashir
L. C. W. University, Lahore, Pakistan

Ghulam Shabbir†
Materials Division, PINSTECH, Islamabad 45650, Pakistan

(Received 2 September 2019 : accepted 31 January 2020)

The Thermal properties of nano-crystalline CeO_2, FeO, MgO, Ho_2O_3, NiO and Y_2O_3, prepared by using the co-precipitation method, have been investigated using X-ray diffraction (XRD) at room temperature. The integrated intensity data obtained from the X-ray diffraction experiments was utilized to determine the temperature factor ($\overline{B(T)}$), mean square amplitude of vibration ($\overline{u^2(T)}$), Debye temperature (θ_D), melting point (T_m) and activation energy for vacancy formation (E_f). The values of ($\overline{B(T)}$) and ($\overline{u^2(T)}$) in the present case were found to be large while the values of θ_D and E_f were found to be lower than the corresponding values reported for the binary oxides with large particle sizes. This suggests that a decrease in particle size from micro to nano-scale may induce weakening of the bonds. On a nano-scale as compared to ordinary size, the values of the melting points were found be higher for the heavier atomic oxides.

PACS numbers: 61.46.−w, 61.05.C−
Keywords: X-ray diffraction, Binary oxides, Thermal properties

I. INTRODUCTION

Cubic binary oxides are of great importance for a number of technological applications such as heterogeneous catalysis, corrosion-protective coating of metals and microelectronic devices etc. [1]. Magnesium oxide (MgO) is a very interesting material with unique applications in the fields of electronics, catalysis, petrochemical industry, as antibacterial agent for water purification, ceramics industry, high temperature insulation and oxide barrier for spin tunneling devices [2,3]. Ceramics are doped with MgO in order to inhibit grain growth that improves fracture toughness [4]. Iron oxide (FeO) [5], nickel oxide (NiO) [6], and yttrium oxide (Y_2O_3) [7], especially in the nano-size range, have attracted much attention of researchers due to their technical applications. Cerium dioxide (CeO_2) is widely applied as an oxygen storage material in automobile exhaust catalysts. Ceria-based materials have been reviewed for their application as an electrolyte in the solid oxide fuel cells [8]. CeO_2 and

*E-mail: hwangkok@hallym.ac.kr
†E-mail: gshabbir@gmail.com

holmium oxide (Ho_2O_3) are used as additives in ceramics in order to enhance the electrical properties of the ceramics [9].

Various thermal parameters of solids, such as characteristic Debye temperature (θ_D), temperature factor ($\overline{B(T)}$), coefficient of thermal expansion and mean square amplitude of vibration ($\overline{u^2(T)}$), are important due to their relation with elastic and thermal properties of solid. The accurate data of such properties is always required not only for crystallographic use but also for the design and optimization of new materials for different industrial applications [10–13]. Further, it is well known that such properties can be tailored, for desired technical applications, by changing the particle size from ordinary to nano-size through a number of soft solution processing techniques [14].

The thermal properties of some binary cubic and alkaline earth oxides with ordinary particle size have been reported in literature [15,16]. A number of methods were used to determine the Debye temperature of MgO including but not limited to: heat capacity measurements [17], temperature dependence of elastic constants from 4.2 K to 300 K [18], elastic neutron scattering data of the powder samples at room temperature [19], and calculations from the elastic moduli, in good agreement with those obtained from sound wave velocity measurements [20]. The energies required for formation of neutral oxygen vacancies have been studied in the single crystals of ultrathin films of some cubic oxides for bulk, sub-surface sites at different depths from surface and various surface sites [21]. The Debye temperature of NiO was determined by heat capacity measurements [22] and elastic constants [23]. The structural properties and elastic constants for CeO_2 have been determined by first principle calculations [24]. Debye temperatures were determined from the average sound wave velocities calculated by local density approximation (LDA) and generalized gradient approximation (GGA) methods [23,24]. The effect of pressure on Debye temperatures of CeO_2 have been investigated via first-principle calculations by using elastic constants which were calculated in the framework of LDA.

The review of literature shows that the oxides used in most of the previous studies had ordinary particle sizes i.e. micro-meter range [25]. The present study is motivated by the fact that changes in particle size are always accompanied by changes in properties of the material. We systematically investigated structural and thermal properties of nano-crystalline CeO_2, FeO, MgO, Ho_2O_3, NiO and Y_2O_3, prepared by co-precipitation method.

II. EXPERIMENTAL METHODS

1. Sample Preparation

The nano-crystalline binary oxides with nominal composition of CeO_2, FeO, MgO, Ho_2O_3, NiO and Y_2O_3, were synthesized by co-precipitation technique. The analytical grade metal salts of $Mg(NO_3)_2$, $Fe(NO_3)_3.9H_2O$, $Ni(CH_3COO)_2.4H_2O$, $Y(NO_3)_3.6H_2O$, $Ce(NO_3)_3.6H_2O$ and $Ho(NO_3)_3.5H_2O$ with appropriate molar ratios were dissolved in deionized water and mixed in a beaker. These solutions were stirred on a hot plate for ∼2 hours and then KCl (0.3M) was added. Then 2M NaOH (as a precipitating agent) was added drop by drop under continued stirring to achieve a pH-value of 12. The stirring process was further continued for 3 hours in order to get the homogeneous distribution of particles in the samples [26]. The precipitates thus obtained were washed with deionized water, dried at ∼373 K for 5 hours and finally annealed at ∼900 K for ∼8 hours. The chemical reaction involved for the preparation of MgO nano-crystalline oxide (as an example) is given below:

$$Mg(NO_3)_2 + 2NaOH \rightarrow Mg(OH)_2 + 2NaNO_3$$

$$Mg(OH)_2 \rightarrow MgO + H_2O$$

A similar procedure was adopted for the preparation of nano-sized powders of other oxides. The X-ray diffraction (XRD) experiments were performed in a step scan mode (with a step of 0.01° and a counting time of 10 s per step) in θ-θ geometry on a Bruker AXS D8 Advance powder diffractometer with nickel filtered CuK_α radiations (λ = 1.5418 Å) generated at 45 kV and 40 mA.

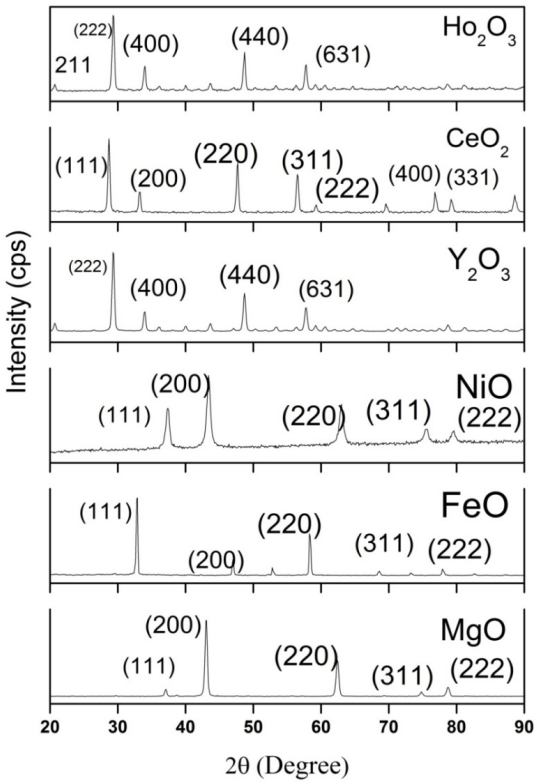

Fig. 1. X-ray diffraction patterns for MgO, FeO, NiO, Y_2O_3, CeO_2 and Ho_2O_3 nanoparticles taken at room temperature.

2. Data Analysis

The crystallite size (D) was calculated from the high-intensity Bragg reflections by using the Scherrer formula [27]:

$$D = \frac{\kappa\lambda}{\beta\cos(\theta)} \tag{1}$$

where $k(\approx 0.9)$ is a shape factor and β is the full width at half maximum in radians at a given 2θ. The Bragg angles for each reflection were determined by using X' Pert HighScore diffraction software. This software enabled deconvolution of the low angle reflections so that $K\alpha_1$ and $K\alpha_2$ lines could be determined accurately. The diffraction patterns shown in Fig. 1 correspond to $K\alpha_1$ wavelength only. The instrumental broadening correction was applied by measuring Si-powder (4N grade) prior to crystallite size determination by means of a 4N-grade silicon powder as an external standard.

The X-ray diffraction patterns were indexed by analytical methods. The true value of lattice parameter 'a' for each sample was determined by the extrapolation of lattice parameters for various reflections against Nelson-Riley function [27]. The integrated intensity of Bragg reflection for a powder specimen is given by:

$$I_{\rm cal} = pLPF^2e^{-2M} \tag{2}$$

where p is the multiplicity factor, LP is the Lorentz-Polarization factor, F is the structure factor and e^{-2M} is the Debye-Waller factor [27]. The relation between $\overline{B(T)}$ and the logarithm of normalized integrated intensity ($I_{\rm obs}/I_{\rm cal}$) is given as follows:

$$\ln(I_{\rm obs}/I_{\rm cal}) = \ln K' - 2\overline{B(T)}(\sin^2\theta/\lambda^2) \tag{3}$$

In this equation, K' is a scale factor. The temperature factor and the mean square amplitude of vibration ($\overline{u^2(T)}$) are related to the Debye temperature (θ_D) in the Debye's high-temperature approximation [27]:

$$\overline{B(T)} = 8\pi^2\overline{u^2(T)} = \left(\frac{6h^2}{mk_{\rm B}}\right)\left(\frac{T}{\theta_D^2}\right) + B_o \tag{4}$$

In Eq.(4), h, T, m and $k_{\rm B}$ are the Planck's constant, absolute temperature, mass of the molecule and Boltzmann constant, respectively, and B_o is the static part of the $\overline{B(T)}$.

The energy for vacancy formation (E_f) for each oxide sample was determined by using the following relation:

$$E_f = A\frac{k_{\rm B}}{h}m\theta_D^2a^2 \tag{5}$$

where A is a constant. The above relation was given by H. R. Glyde [28] and its validity has been proven for several face-centered cubic (fcc), body centered cubic (bcc) and hexagonal close packed (hcp) materials.

The melting point T_m for each oxide sample was determined by using the Lindemann's formula [29]:

$$T_m = \frac{x_m^2}{9h^2}mk_{\rm B}\theta_D^2r_s^2 \tag{6}$$

where, $x_m \approx 0.2 - 0.25$ for most solid materials and r_s is the mean radius of the unit cell.

III. RESULTS AND DISCUSSION

X-ray diffraction patterns for nano-crystalline Ho_2O_3, CeO_2, Y_2O_3, NiO, FeO and MgO are shown in Fig. 1.

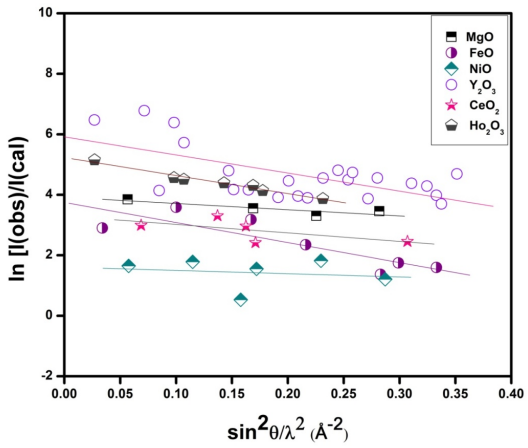

Fig. 2. (Color online) Wilson plots for MgO, FeO, NiO, Y_2O_3, CeO_2 and Ho_2O_3 nanoparticles.

It was found that MgO, FeO, NiO and CeO_2 have fcc structure whereas, Y_2O_3 and Ho_2O_3 have bcc structure. The value for $\overline{B(T)}$ was obtained from the slope of the plot of $\ln(I_{\rm obs}/I_{\rm cal})$ against $\sin^2\theta/\lambda^2$ which is known as Wilson plot. Figure 2 shows the result. The observed values of $\overline{B(T)}, \overline{u^2(T)}, \theta_D$, melting point ($T_m$) and E_f as determined by X-ray diffraction experiments are given in Table 1 (where a, b, c, d, e, f, and g correspond to references [15], [16], [30], [31], [21], [32], and [22], respectively).

It is pertinent to mention that use of diffraction data to calculate crystallite size is more reliable than other techniques such as scanning electron microscopy (SEM) because of the fact that it is not possible to determine crystallite size of an individual crystallite in an agglomerated grain. However, SEM micrographs were also taken to study grain size and morphology. The results are shown in Fig. 3(a-e). CeO_2 particles have been found to be rounded agglomerates (Fig. 3a), whereas, FeO (Fig. 3b) and Ho_2O_3 (Fig. 3c) are cubic with well-defined boundaries. The SEM micrographs for Y_2O_3 and NiO are shown in Fig 3d and 3e, respectively. The particles are round in shape while in NiO, small particles combine with each other and form a mesosphere like morphology as shown in Fig. 3e (inset).

The sizes of the particles are in 50 – 70 nm range, which is in agreement with the XRD data while the mesospheres for NiO are in the 1– 2 μm range and, as already

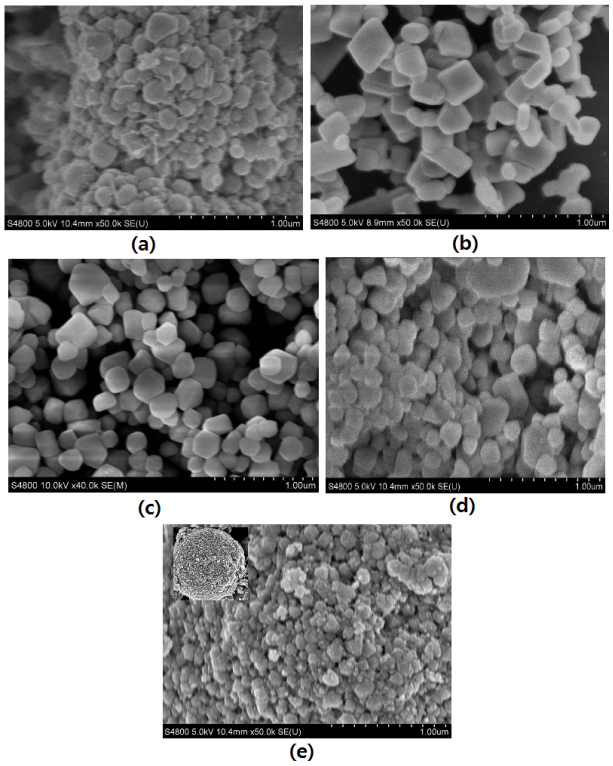

Fig. 3. SEM micrographs for (a) CeO (b) FeO (c) Ho_2O_3 (d) Y_2O_3 (e) NiO nanoparticles.

explained, cannot be resolved to the individual crystallite size under a microscope.

The values for $\overline{B(T)}$ and $\overline{u^2(T)}$ were found to be higher for MgO and CeO_2 nanoparticles than the reported values [15, 16, 32]. On the other hand, the values for θ_D for MgO, NiO and CeO_2 nanoparticles are found to be smaller as compared to the reported values [16, 22, 30, 32]. Debye temperature is the material physical parameter that is associated with the bond strengths between atoms of the material. The higher the value of θ_D, the stronger the bonding between atoms. A decrease in the value of θ_D indicates that the bonding between the atoms is reduced which is in accordance with the increase of the temperature factor with the reduction in size of crystallites to nanometer size. When the size of the crystallites reduces, atomic vibrations increase resulting in the weakening of the interatomic bonding. Since θ_D is associated with the stiffness of the materials, it is concluded that the material gets softer as the size of the crystallites is reduced to nanoscale. Melting point is observed to decrease in case of MgO and FeO nanoparticles, whereas, it is observed to increase in the case of NiO, Y_2O_3, CeO_2

Table 1. The values for lattice parameter (a), crystallite size, temperature factor ($\overline{B(T)}$), mean square amplitude of vibration ($\overline{u^2(T)}$), Debye temperature (θ_D), melting point (T_m) and activation energy for vacancy formation (E_f) determined by X-ray diffraction experiments.

Sample	Lattice parameter a (Å)	Crystallite size (nm)	$\overline{B(T)}$ (Å^2)	$\overline{u^2(T)}$ (Å^2)	θ_D (K)	T_m (K)	E_f (eV)
MgO	4.217±0.001	21.7±0.20	0.994±0.10 0.350[a]	0.013 0.004[b]	414±2 697.0[b] 939.1[c]	2177 3125[d]	1.29 10.08[e]
FeO	4.105±0.002	28.1±0.12	1.408±0.05	0.018	260±4	1456 1650[d]	0.86
NiO	4.179±0.001	21.7±0.18	0.542±0.07	0.007	412±2 404.0[f] 595(20)[g]	3921 2228[d]	2.32
Y_2O_3	10.611±0.003	20.9±0.10	3.352±0.11	0.042	150±3	4087 2450[d]	2.42
CeO_2	5.413±0.002	20.8±0.09	1.210±0.03 0.490[f]	0.015 0.006[f]	222±5 354.0[g]	2947 2698[d]	1.74
Ho_2O_3	10.622±0.002	20.8±0.10	2.169±0.20	0.027	145±4	6328 2688[d]	3.74

[a]Ref.15, [b]Ref.16, [c]Ref.30, [d]Ref.31, [e]Ref.21, [f]Ref.32, [g]Ref.22

and Ho_2O_3 nanoparticles. The values of these thermal properties are reported for the first time for FeO, Y_2O_3 and Ho_2O_3 nanoparticles in this study.

The vacancy generation is a dominant feature for diffusion mostly in pure form of metals as well as substitutional solid solutions, so the values for the energy for vacancy formation are helpful in understanding the process of diffusion in the substitutional solid solutions. Therefore, an attempt was made to estimate the values of the energy of vacancy formation (E_f) for MgO, FeO, NiO, Y_2O_3, CeO_2 and Ho_2O_3 nanoparticles by using Eq. (5). The data regarding E_f is available in literature only for MgO [21]. It is observed that, as the particle size decreases to nanometers, the θ_D is reduced which reveals that the bond strength between atoms is reduced and it becomes easier to produce vacancies at low energies. For CeO_2, NiO, FeO, Ho_2O_3, and Y_2O_3 oxides, E_f values are reported for the first time in the nanometer-sized range whereas already published data on these selected oxides are with ordinary size (micrometer range).

On the basis of results obtained in the present study, it can be accomplished that these materials may have a potential for various applications such as heterogeneous catalysis, corrosion-protective coating of metals and microelectronic devices, high temperature insulation and oxide barrier for spin tunneling devices etc.

IV. CONCLUSION

In order to investigate the structural and thermal properties of six selected cubic binary oxides (i.e. MgO, FeO, NiO, Y_2O_3, CeO_2 and Ho_2O_3), X-ray diffraction studies have been carried out at room temperature. From the results, it is concluded that the values for lattice parameters determined in this study are in good agreement to those available in literature for all investigated binary oxides. It is determined that the values of temperature factor and mean square amplitude of vibration increase as the size of the crystallites is reduced to nanometer range. The values for Debye temperature and activation energy for vacancy formation are reduced from that provided in literature which shows that the bonds get weaker at nanometer scale as compared to ordinary size crystallites. It is observed that the value for melting point is reduced for lighter atom oxides while it is increased in the case of heavier atoms at nanoscale as compared to ordinary size crystallites.

ACKNOWLEDGEMENTS

This study was supported by the National Research Foundation of Korea (NRF) grant funded by the Korea government (MSIP, NRF – 2019R1H1A2079858).

REFERENCES

[1] M. V. G. Pirovano, A. Hofmann and J. Sauer, Sur. Sci. Reports **62**, 219 (2007).

[2] M. R. Bindhu *et al.*, Mater. Lett. **166** 19 (2016).

[3] I. O. Wilson, IEEE Proc. **128A**, 159 (1981).

[4] C. Y. Tan *et al.*, Ceram. Int. **39**, 8979 (2013).

[5] H. I. Adegoke, F. A. Adekola, O. S. Fatoki and B. J. Ximba, Pol. J. Environ. Stud. **22**, 7 (2013).

[6] M. N. Rifaya, T. Theivasanthi and M. Alagar, Nanosci. and Nanotech. **2**, 134 (2012).

[7] V. Swamy, N. A. Dubrovinskaya and L. S. Dubrovinsky, J. Mater. Res. **14**, 456 (1999).

[8] M. Yashima *et al.*, Chem. Phys. Lett. **372**, 784 (2003)..

[9] P. Fu *et al.*, J. Mater. Sci.: Mat. Elect. **23**, 2167 (2012).

[10] N. M. Butt, J. Bashir, B. T. M. Willis and G. Heger, Act. Cryst. A **44**, 396 (1988).

[11] N. M. Butt, J. Bashir and M. N. Khan, Act. Cryst. A **49**, 171 (1993).

[12] N. M. Butt, J. Bashir, M. N. Khan and B. T. M. Willis, J. Mater. Sci. Lett. **13**, 1440 (1994).

[13] J. Bashir, N. M. Butt and Q. H. Khan, Act. Cryst. A **44**, 638 (1988).

[14] G. Shabbir, A. H. Qureshi and K. Saeed, Mater. Lett. **60**, 3706 (2006).

[15] G. V. Valat, J. P. Vidal and K. K. Suonio, Act. Cryst. A **34**, 594 (1978).

[16] R. K. Gupta, Phys. Rev. B **12**, 4452 (1975).

[17] T. H. K. Barron, W. T. Berg and J. A. Morrison, Proc. Roy. Soc. London A **250**, 70 (1959).

[18] K. Marklund and S. A. Mahmoud, Phys. Scripta **3**, 75 (1971).

[19] M. M. Beg, Act. Cryst. A **32**, 154 (1976).

[20] R. Freer, J. Mater. Sci. **16**, 3225 (1981).

[21] J. Carrasco, N. Lopez, F. Illas and H. –J. Freund, J. Chem. Phys. **125**, 074711 (2006).

[22] H. Seltz, B. J. Dewitt and H. J. McDonal, J. Amer. Chem. Soc. **62**, 88 (1940).

[23] C. Loschen, J. Carrasco, K. M. Neyman and F. Illas, Phys. Rev. B **75**, 035115 (2007).

[24] P. Haas, F. Tran and P. Blaha, Phys. Rev. B **79**, 085104 (2009).

[25] L. L. Sun, Y. Cheng and G. –F. Ji, J. At. Mol. Sci. **1**, 143 (2010).

[26] M. N. Ashiq, M. J. Iqbal and I. H. Gul, J. Alloys. Compd. **487**, 341 (2009).

[27] B. D. Cullity 1978 Elements of X-ray Diffraction 2nd edn (Reading, MA: Addison-Wesley)

[28] H. R. Glyde, J. Phys. Chem. Solids **28**, 2061 (1967).

[29] J. M. Ziman 1969 Principles of the Theory of Solids (Cambridge University Press)

[30] W. H. White, J. Chem. Phys. **61**, 4907 (1974).

[31] SpringerMaterials, https://materials.springer.com/lb/docs/sm_lbs_978-3-540-31359-5_215

[32] T. O. Baldwin and C. W. Tompson, J. Chem. Phys. **41**, 1420 (1964).

[33] S. V. Suryanarayana and J. Sadanandam, Ind. J. Pure and Appl. Phys. **14** (1974) 780.